Annals of Glaciology 20 1994

Numerical flow simulation at local parts of Filchner–Ronne Ice Shelf, Antarctica

M. JONAS*, K. GROSFELD AND F. THYSSEN
Institut für Geophysik, Forschungsstelle für physikalische Glaziologie der Westfälischen Wilhelms-Universität Münster, D-48149 Münster, Germany

ABSTRACT. The Münster radio-echo-sounding (RES) work in the central part of Filchner–Ronne Ice Shelf has revealed new information. Different signatures are discernible in the airborne RES data. Local model calculations in the area between Henry Ice Rise and Berkner Island are used to interpret these signatures in terms of thermal and dynamic parameters. From our airborne measurements, the shapes of the meteoric and marine-ice layers were prepared as input data for dynamic-model calculations. A general increase in the temperature-dependent flow parameter is compared with a spatially variable flow parameter that is derived from model calculations concerning freezing and melting processes. Velocity and strain fields were calculated by a finite-difference method on a local data base between Henry Ice Rise and Berkner Island.

INTRODUCTION

One of the major factors which determine the flow of an ice shelf is its temperature, T, through its influence on the flow parameter in the Arrhenius equation $A(T') = A_0 \exp(-Q/RT')$. A_0 represents a constant, R is the gas constant, T' is the absolute temperature and Q is the activation energy. The temperature distribution within an ice shelf depends on the temperature at the ice surface, the water temperature at the ice-shelf bottom, the accumulation and melting rates, and the temperature distribution within the ice streams discharging into the ice shelf. These environmental conditions vary at different regional and local situations. Consequently, the ice body produces local and regional structural features. These features are illustrated in the Glaciological Map of Filchner–Ronne Ice Shelf (Swithinbank and others, 1988). In addition, the distributions of meteoric and marine ice were determined from radio-echo sounding and elevation measurements in the central part of Filchner–Ronne Ice Shelf and were compiled together with recognizable structural marks derived from airborne RES by Thyssen and others (1992). In both maps, a zone of "chaotic disturbed" or "destroyed meteoric ice" northeast of Henry Ice Rise is described. Diffraction hyperbolas, found in high-resolution RES measurements (Blindow, 1991), follow distinct flowlines which partly originate in this area (Blindow, 1994). One reason for the crevassing is the grounding zone of Henry Ice Rise (see Fig. 1). Another reason is the formation of the marine ice layer due to crystallization processes in the water column

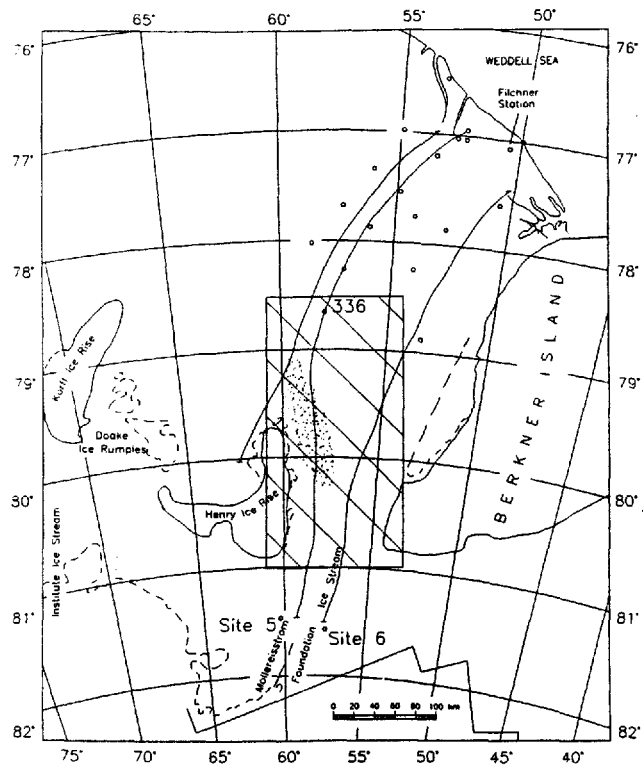

Fig. 1. Flowlines for the thermal modeling, geodetic points (Möller and others, 1992) and location of the data base for local dynamic model calculations (rectangular box in middle of figure). The disturbed ice is marked with a dotted field (map from Swithinbank and others, 1988).

* Present address: Institut für Angewandte Geodäsie, D-6000 Frankfurt am Main 70, Germany.

https://doi.org/10.3189/1994AoG20-1-391-396 Published online by Cambridge University Press

beneath the central part of Filchner Ronne Ice Shelf (Thyssen, 1986, 1988, 1991; Engelhardt and Determann, 1987; Oerter and others, 1992).

The area of marine ice covered by this study is limited by Rutford Ice Stream in the west, Korff Ice Rise and Henry Ice Rise with Doake Ice Rumples in the south and Foundation Ice Stream in the east (Thyssen and others, 1992).

Heat advection due to marine accumulation is the main reason for the increase of the ice temperature and therefore for the flow parameter. Spatially varying flow parameters derived from the vertical temperature distributions observed in boreholes and thermal model calculations along selected flowlines, assuming steady state (Grosfeld, 1992), are employed in two-dimensional flow simulations. This leads to a local maximum of vertically integrated temperature which is calculated to occur north and northeast of Henry Ice Rise between 150 and 200 km along the flowline downstream of Möller-eisstrom (Grosfeld, 1992). We therefore have a condition of confined flow between Henry Ice Rise and Berkner Island coupled with horizontal temperature variations. In this paper a local flow simulation with a horizontally varying flow parameter is compared with conventional calculation using a constant flow parameter.

THEORY

Model calculations on Filchner–Ronne Ice Shelf with two-dimensional finite-element methods (Lange and MacAyeal, 1986, 1988) or finite-difference methods (Determann, 1991a) were conducted on a Filchner–Ronne Ice Shelf data base. We used a versatile finite-difference method, developed for local data bases with high resolutions. For the descriptions, λ, ϕ, z are used as coordinates on a polar stereographic projection, x, y, z as position components and u, v, w as velocity components. Flow simulations are based on the numerical solution of the momentum equations under ice-shelf conditions. With stress tensor $\vec{\sigma}$, ice density ρ, gravitational acceleration g and vertical unity vector $\vec{k}$, neglecting inertial forces and the Coriolis force, the equation of motion can be written (Lliboutry, 1987) as:

$$\nabla \cdot \vec{\sigma} \rho g \vec{k} = 0 . \tag{1}$$

The generalized flow law for incompressible material (Jaeger, 1969): $\dot{\epsilon}_{xy} = A\sigma^{n-1}\sigma'_{xy}$ with $\dot{\epsilon}_{xy}$ the strain-rate components, σ'_{xy} the stress-deviator components, σ the effective stress, n the flow-law exponent ($n = 3$) and A the flow parameter, depending on temperature T (Paterson, 1981), describes the relation between deformation rate and the stress tensor.

Looking at the ice-shelf flow as deforming ice columns, vertical shear is negligible (Sanderson and Doake, 1979), so that $\delta\sigma'_{xz}/\delta x, \delta\sigma'_{yz}/\delta y = 0$. A vertically integrated flow parameter

$$\bar{A}(T(x,y)) = \left[\int_{z_{\text{bottom}}}^{z_{\text{surface}}} A(T(x,y,z))^{-1/n} \mathrm{d}z \right]^{-n} \tag{2}$$

can be derived from temperature distribution. Vertical deformation can be taken into account by using ice equivalent for vertical density variation (Thyssen, 1988). The velocity change with flow parameter is considered in the flow law with u, v, w as velocity components

$$\dot{\epsilon}_{ij} = \frac{1}{2}\left(\frac{\delta u}{\delta x_i} + \frac{\delta v}{\delta x_j}\right). \tag{3}$$

Using Equations (2) and (3), the elliptic differential equations of second order can be solved with the surface-elevation gradients $\delta z/\delta x$, $\delta z/\delta y$ to:

$$\begin{aligned}
&-\rho g \frac{\delta z}{\delta x} A(x,y)^{1/n} = \\
&2\frac{\delta}{\delta x}\left(f\left(\frac{\delta u}{\delta x}\right)\right) + \frac{\delta}{\delta x}\left(f\left(\frac{\delta v}{\delta y}\right)\right) + \frac{1}{2}\frac{\delta}{\delta y}\left(f\left(\frac{\delta u}{\delta y} + \frac{\delta v}{\delta x}\right)\right), \\
&-\rho g \frac{\delta z}{\delta y} A(x,y)^{1/n} = \\
&2\frac{\delta}{\delta y}\left(f\left(\frac{\delta v}{\delta y}\right)\right) + \frac{\delta}{\delta y}\left(f\left(\frac{\delta u}{\delta x}\right)\right) + \frac{1}{2}\frac{\delta}{\delta x}\left(f\left(\frac{\delta u}{\delta y} + \frac{\delta v}{\delta x}\right)\right).
\end{aligned} \tag{4}$$

With $\delta u/\delta z$, $\delta v/\delta z \approx 0$ and $\delta w/\delta x$, $\delta w/\delta y \ll \delta u/\delta x$, $\delta v/\delta y$, f and the effective strain rate is calculated:

$$\begin{aligned}
f &= \left[\frac{1}{2}\left(\frac{\delta u^2}{\delta x^2} + \frac{\delta v^2}{\delta y^2} + \frac{\delta u^2}{\delta z^2}\right) + \frac{1}{4}\left(\frac{\delta u}{\delta y} + \frac{\delta v}{\delta x}\right)^2\right]^{-(1-(1/n))/2} \\
&= \dot{\epsilon}^{(1/n)-1} .
\end{aligned} \tag{5}$$

The velocity components were approximated with difference forms of Equations (2) and (3), comparable to diagnostic procedures described by Determann (1991b). Looking at the approximated velocity components as dilatation parameters, principal strain rates were calcul-ated to compare with geodetically measured strain rates. $e_{1,2} = \frac{1}{2}(\dot{\epsilon}_{xx} + \dot{\epsilon}_{yy} \pm \bar{e})$ with $\bar{e} = \sqrt{(\dot{\epsilon}_{xx} - \dot{\epsilon}_{yy})^2 + 4\dot{\epsilon}_{xy}}$ (Möller and others, 1992). The vertical strain rate $\dot{\epsilon}_{zz} = -(\dot{\epsilon}_{xx} + \dot{\epsilon}_{yy}) = -(e_1 + e_2)$ can be determined as invariant under transformation of the coordinate system. Together with the flow law, stress-deviator components can be calculated with $\sigma'_{ij} = \dot{\epsilon}_{ij} A^{-1/n} \dot{\epsilon}^{1-(1/n)}$.

The theoretical basis of the temperature calculation is heat conduction and advection with thermal properties, depending on density, salinity and temperature. The method has been described in detail for the flowline downstream of Möllereisstrom by Grosfeld and Thyssen (1994). The vertical temperature distribution $T(\lambda, \phi, z)$ is calculated using ice thickness $H = H_{\text{meteoric}} + H_{\text{marine}}$, velocity, melting and freezing rate, and top and bottom temperature at 2 km grid intervals along the flowlines in Figure 1 and equidistant vertical increments between 4 m and about 1 m. These temperature values were used to calculate the appropriate flow parameter (Paterson, 1981) and vertically integrated to get $\bar{A}(\lambda, \phi)$, which was transformed to the x, y coordinate system. For the dynamic simulation, this flow parameter $\bar{A}(x, y)$ and the ice thickness $H(x, y)$ are used as input data.

https://doi.org/10.3189/1994AoG20-1-391-396 Published online by Cambridge University Press

DATA BASES AND RESULTS

An interactive program system was created on a personal computer to approximate velocity components at each grid point using a finite-difference relaxation method and to calculate the strain-rate components and stress-deviator components. In the central part of Filchner Ronne Ice Shelf, ice-thickness distributions H, H_{meteoric} and H_{marine} have been derived from airborne RES measurements together with elevation measurements along flight tracks (Thyssen and others, 1993). Two-dimensional data sets were calculated by mathematical tool programs for gridding and interpolation. Ice thickness, constructed in the central area with grid distances of 10 km in the x direction and 13 km in the y direction, was used for regional model calculations with an average flow parameter of $A = 7.5 \times 10^{-18}$ Pa^{-3} a^{-1} (Determann, 1991a) to derive the boundary conditions for the local grid. The results are shown in Figure 2.

Compared to the results of Determann (1991a), the velocities are decreased due to boundary conditions which consider two components of the strain rate at the ice front (Huybrechts, 1992). Thus, deviations of grid-point positions from the actual coastline may decrease the accuracy of the model results. The model predictions are in reasonable agreement with the geodetically measured velocities. Near site 5 (Fig. 1), the results show velocities between 100 and 200 m a^{-1} compared to 170 (Ritter and Karsten, 1991) and 198.5 m a^{-1} (Morris and Vaughan, 1991). At point 336, the model velocity reaches 600 m a^{-1}, where 660 m a^{-1} (Möller and others, 1992) was measured.

Downstream of Möllereisstrom and Foundation Ice Stream, the data base for an area between Henry Ice Rise and Berkner Island, 140 km wide and 280 km long, was prepared. It is marked in Figure 1 together with the flowlines used for modeling of $(T(\lambda, \phi))$ (Thyssen and others, 1993; Grosfeld and Thyssen, 1994). The data bases of ice thickness and flow parameter are converted to grid distances of 1.4 km. They are shown in Figure 3

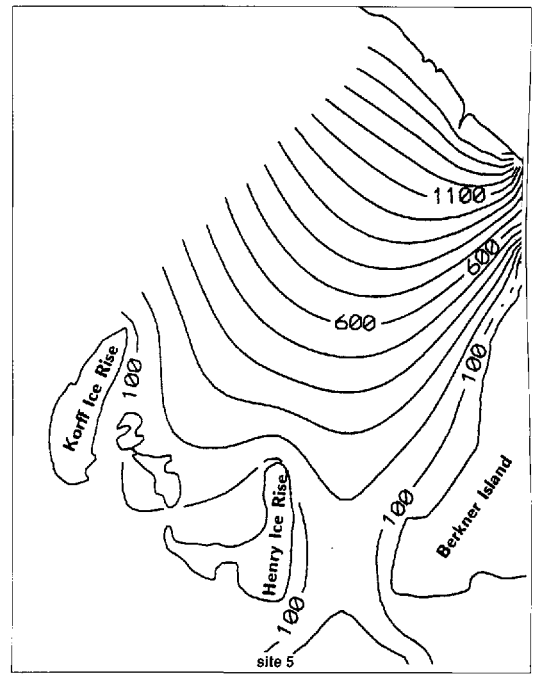

Fig. 2. Velocities in m a^{-1} of regional calculation for the boundary values (map from Swithinbank and others, 1988).

together with the thickness of the marine-ice layer in this area. The derived integrated flow parameter at Foundation Ice Stream, where no basal freezing has been detected, ranges between 4.4×10^{-18} and 7.5×10^{-18} Pa^{-3} a^{-1}, corresponding to temperatures between $-22.5°$ and $-17.5°$C. In the area of marine ice, $\bar{A}$ varies from 1×10^{-17} to 3.5×10^{-17} Pa^{-3}a^{-1}, which corresponds to average temperatures between $-15°$ and $-7.5°$C.

A local maximum of 3.3×10^{-17} Pa^{-3} a^{-1} is reached north and northeast of Henry Ice Rise. As expected, the flow parameter reaches a local maximum in this area of

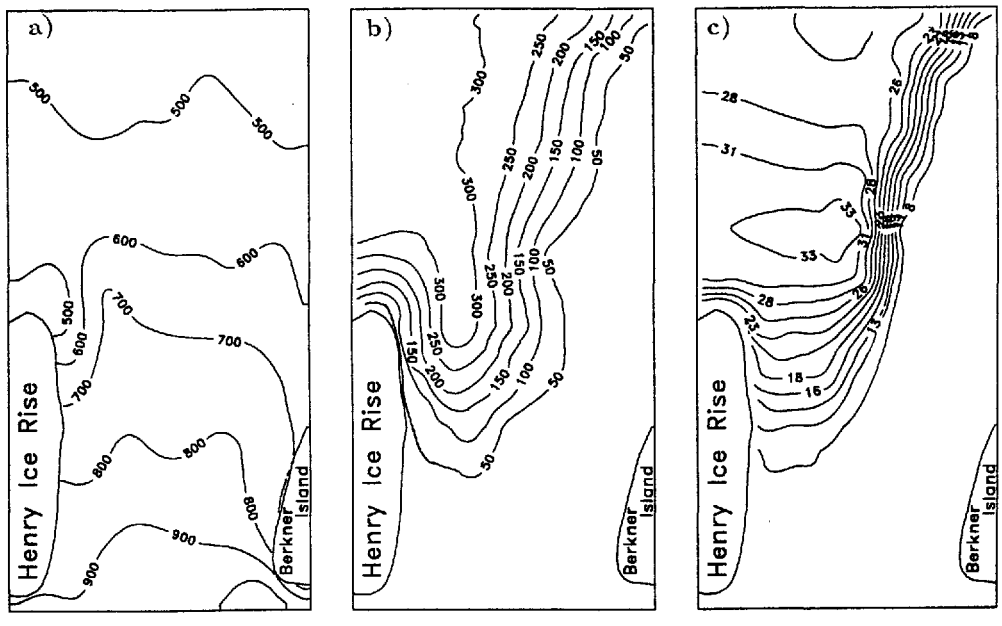

Fig. 3. Data bases of (a) ice thickness H (m), (b) marine-ice thickness H_{marine} (m) (Thyssen and others, 1993) and (c) flow parameter $\bar{A}$ ($\times 10^{-18}$ Pa^{-3} a^{-1}).

https://doi.org/10.3189/1994AoG20-1-391-396 Published online by Cambridge University Press

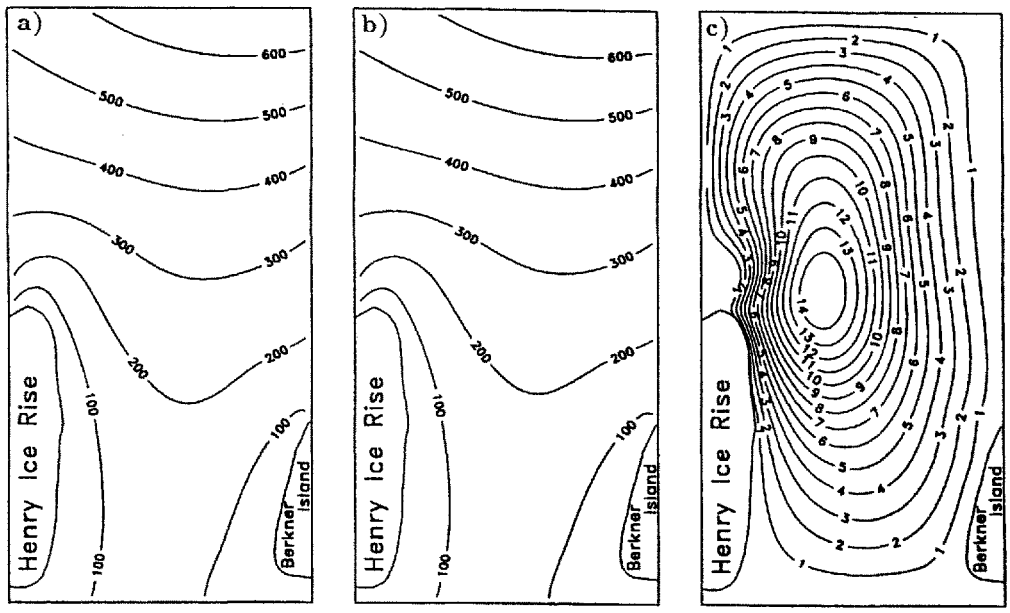

Fig. 4. Velocities in $m\,a^{-1}$ of calculation with (a) $A(T(x,y))$ (Fig. 3c), (b) constant-flow parameter of $7.5 \times 10^{-18}\,Pa^{-3}\,a^{-1}$, (c) difference between (a) and (b).

basal freezing (Grosfeld and Thyssen, 1994).

On the local domain, two diagnostic simulations were performed. In the first simulation, a spatially variable flow parameter was used. The second one was calculated with the constant-flow parameter of $\bar{A} = 7.5 \times 10^{-18}$ $Pa^{-3}\,a^{-1}$ to get the results on the same grid size. Velocities from both simulations together with the difference are plotted in Figure 4. Even though the boundary values remain unchanged, the difference increases to $14\,m\,a^{-1}$ in the region of basal freezing.

The principal strain rate e_1 at point 336 is measured as $0.0022\,a^{-1}$ (Ritter and Karsten, 1991). The calculated principal strain rates e_1 are shown in Figure 5. In the region of point 336 they reach values between 0.002 and $0.003\,a^{-1}$. Measured and calculated strain rates are comparable in magnitude. The differences are caused by the boundary velocity field and its deviations from measured velocity as described above. The highest values are reached in the grounding zones, decreasing to the region of free-floating ice. The difference diagram shows a local maximum of $0.0004\,a^{-1}$ northeast of Henry Ice Rise. The contribution of the spatially varying flow parameter can be estimated as up to 10%.

The situation is similar, when looking at the vertical strain rates (Fig. 6). A local maximum can be seen northeast of Henry Ice Rise. It is enlarged in the diagram of the spatially varying flow parameter. This area can be identified with the crevassed area (see Fig. 1). Crevassing in this area takes place at the surface. So the temperature of the meteoric ice must be taken into account for the

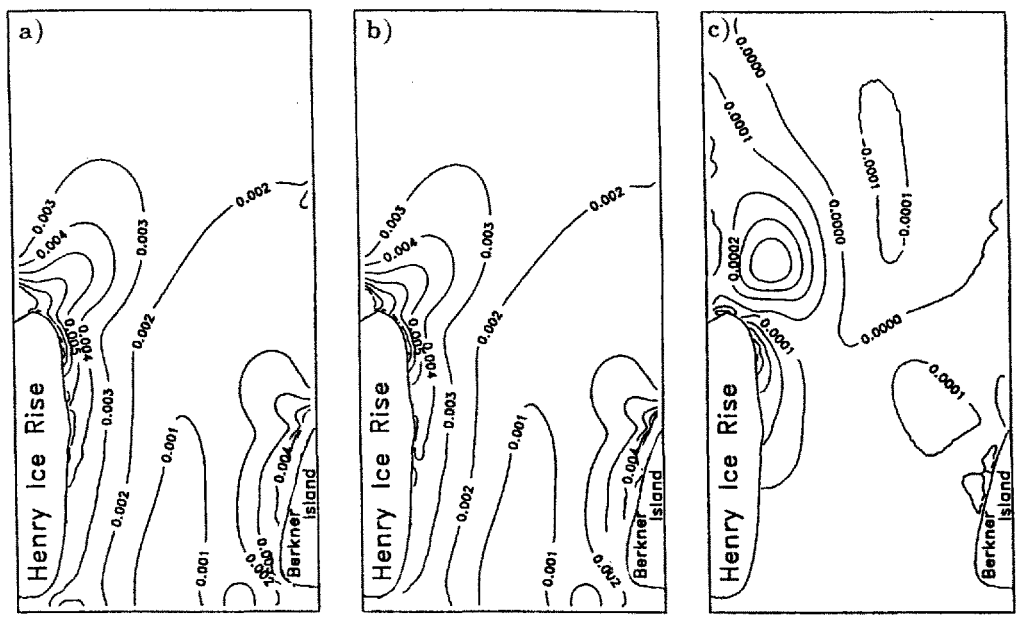

Fig. 5. Principal strain rates e_1 (a^{-1}) of calculation with (a) $A(T(x,y))$ (Fig. 3c), (b) constant-flow parameter of $7.5 \times 10^{-18}\,Pa^{-3}\,a^{-1}$, (c) difference between (a) and (b).

https://doi.org/10.3189/1994AoG20-1-391-396 Published online by Cambridge University Press

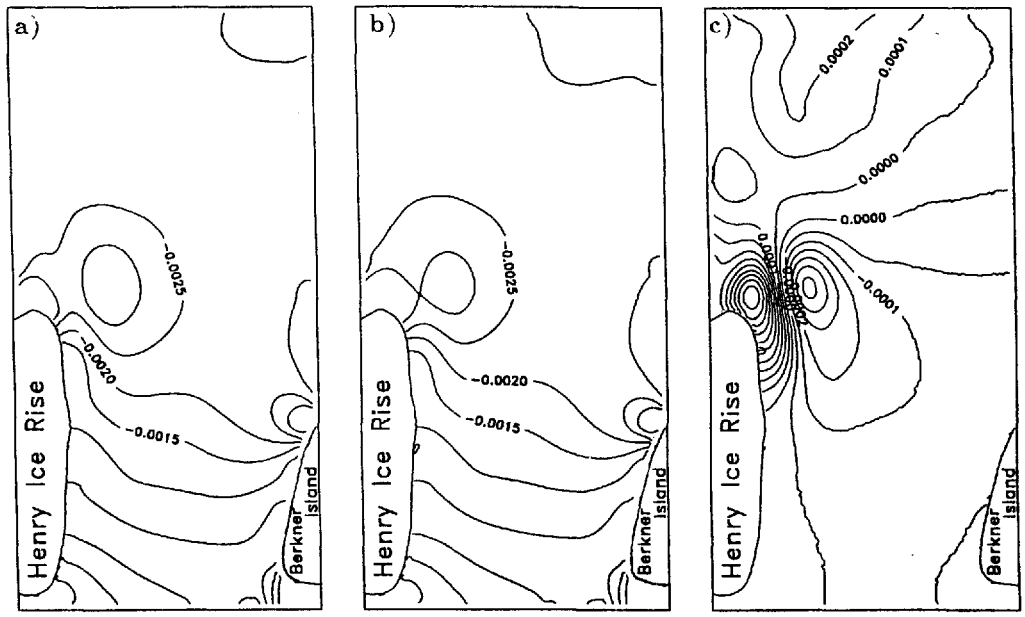

Fig. 6. Vertical strain rates $\dot{\epsilon}_{zz}$ (a^{-1}) of calculation with (a) $A(T(x,y))$ (Fig. 3c), (b) constant-flow parameter of 7.5×10^{-18} Pa^{-3} a^{-1}, (c) difference between (a) and (b).

calculation of the stress components. The principal stress σ_1' in Figure 7 is calculated using a flow parameter of 5.7×10^{-18} Pa^{-3} a^{-1}. The contribution of the temperature increase can be estimated when looking at the differences between the calculation using constant A and lateral-varying $A(T(x,y))$, which is locally increased here. Critical values for crevasses are given as greater than 100 kPa (Weertmann, 1980). They are reached northeast of Henry Ice Rise, if a temperature appropriate to near-surface ice of 20°C is considered.

CONCLUSIONS

The radio-echo-sounding work in the central area of Filchner–Ronne Ice Shelf revealed new information on total ice thickness, meteoric and marine-ice thickness and structural features. These data give information about regional and local situations in more detail and represent a broad base for experimental and numerical procedures. This paper deals with the zone of disturbed ice northeast of Henry Ice Rise. In this area, the values of velocity and vertical strain rates calculated using the spatial-varying flow parameter are up to 10% higher than the values obtained by using a constant-flow parameter. The maxima are situated northeast of Henry Ice Rise. This can be identified with the crevassed area from the satellite map (Swithinbank and others, 1988) and the feature map from Thyssen and others (1993). The increase in the temperature field due to basal accumulation leads to an

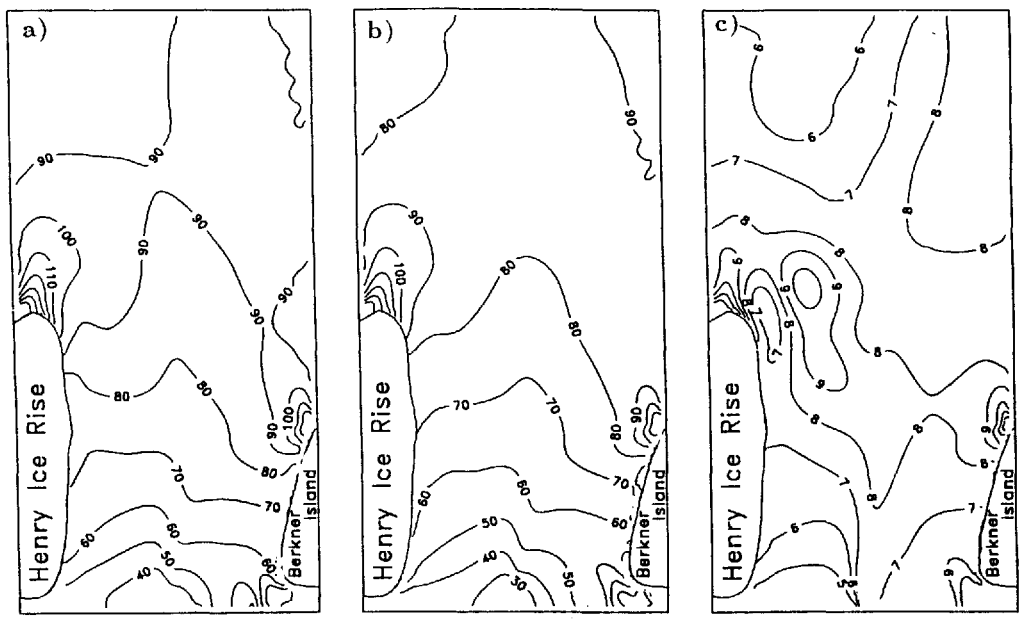

Fig. 7. Near-surface stress component σ_1' (kPa) of calculation with (a) constant-flow parameter of 7.5×10^{-18} Pa^{-3} a^{-1}, (b) $A(T(x,y))$ (Fig. 3c), (c) difference between (a) and (b).

https://doi.org/10.3189/1994AoG20-1-391-396 Published online by Cambridge University Press

enlarged zone of increased vertical strain and accentuates crevassing.

ACKNOWLEDGEMENT

The authors wish to express their thanks to the Deutsche Forschungsgemeinschaft.

REFERENCES

Blindow, N. 1991. Structural features in the central part of the FRIS. *In* Miller, H. and H. Oerter, *eds. Filchner–Ronne-Ice-Shelf-Programme. Report No. 5.* Bremerhaven, Alfred Wegener Institute for Polar and Marine Research, 12.

Blindow, N. 1994. The central part of the Filchner–Ronne Ice Shelf, Antarctica: internal structures revealed by 40 MHz monopulse RES. *Ann. Glaciol.*, **20** (see paper in this volume).

Determann, J. 1991a. Numerical modelling of ice shelf dynamics. *Antarct. Sci.*, **3**(2), 187–195.

Determann, J. 1991b. The flow of ice shelves — numerical simulations using the finite-difference method. *Ber. Polarforsch.* 83.

Engelhardt, H. and J. Determann. 1987. Borehole evidence for a thick layer of basal ice in the central Ronne Ice Shelf. *Nature*, **327**(6120), 318–319.

Grosfeld, K. 1992. *Untersuchungen zu Temperaturregime und Massenhaushalt des Filchner–Ronne-Schelfeises, Antarktis, unter besonderer Berücksichtigung von Anfrier- und Abschmelzprozessen.* Münster, Institut für Geophysik der Westfälischen Wilhelms-Universität.

Grosfeld, K. and F. Thyssen. 1994. Temperature investigation and modeling on the Filchner–Ronne Ice Shelf. Antarctica. *Ann. Glaciol.*, **20** (see paper in this volume).

Huybrechts, P. 1992. The Antarctic ice sheet and environmental change: a three-dimensional modelling study. *Ber. Polarforsch.* 99.

Jaeger, J. C. 1969. *Elasticity, fracture and flow with engineering and geological applications.* London, Methuen.

Lange, M. A. and D. R. MacAyeal. 1986. Numerical models of the Filchner Ronne Ice Shelf: an assessment of reinterpreted ice thickness distributions. *J. Geophys. Res.*, **91**(B10), 10,457–10,462.

Lange, M. A. and D. R. MacAyeal. 1988. Numerical models of steady-state thickness and basal ice configurations of the central Ronne Ice Shelf, Antarctica. *Ann. Glaciol.*, **11**, 64–70.

Lliboutry, L. 1987. *Very slow flows of solids: basics of modeling in geodynamics and glaciology.* Dordrecht, Martinus Nijhoff Publishers.

Möller, D., B. Riedel and B. Ritter. 1992. Strain and velocity determination on Ronne Ice Shelf. *In* Oerter, H. *ed. Filchner–Ronne-Ice-Shelf-Programme. Report No. 6.* Bremerhaven, Alfred Wegener Institute for Polar and Marine Research, 61–68.

Morris, E. M. and D. G. Vaughan. 1991. Glaciological measurements on the southern Ronne Ice Shelf. *In* Miller, H. and H. Oerter, *eds. Filchner–Ronne-Ice-Shelf-Programme Report No. 5.* Bremerhaven, Alfred-Wegener-Institute for Polar and Marine Research, 37–44.

Oerter, H. *and 6 others.* 1992. Evidence for basal marine ice in the Filchner–Ronne Ice Shelf. *Nature*, **358**(6385), 399–401.

Paterson, W. S. B. 1981. *The physics of glaciers. Second edition.* Oxford, etc., Pergamon Press.

Ritter, B. and A. Karsten. 1991. Massenhaushalt und Dynamik des Filchner–Ronne-Schelfeises. Geodäsie. *Ber. Polarforsch.* 86, 50–57.

Sanderson, T. J. O. and C. S. M. Doake. 1979. Is vertical shear in an ice shelf negligible? *J. Glaciol.*, **22**(87), 285–292.

Swithinbank, C., K. Brunk and J. Sievers. 1988. A glaciological map of Filchner–Ronne Ice Shelf, Antarctica. *Ann. Glaciol.*, **11**, 150–155.

Thyssen, F. 1986. The central part of the Filchner/Ronne Ice Shelf. *In* Kohnen, H., *ed. Filchner–Ronne-Ice-Shelf-Programme. Report No. 3.* Bremerhaven, Alfred Wegener Institute for Polar and Marine Research, 81–83.

Thyssen, F. 1988. Special aspects of the central part of Filchner–Ronne Ice Shelf, Antarctica. *Ann. Glaciol.*, **11**, 173–179.

Thyssen, F. 1991. Massenhaushalt und Dynamik des Filchner–Ronne-Schelfeises. Flugprogramm auf dem Filchner/Ronne-Schelfeis und Berkner Island. *Ber. Polarforsch.* 86, 77–79.

Thyssen, F., A. Bombosch and H. Sandhäger. 1993. Elevation, ice thickness and structural mark maps of the central part of the Filchner–Ronne Ice Shelf. *Polarforschung*, **62**(1), 1992, 17–26.

Weertman, J. 1980. Bottom crevasses. *J. Glaciol.*, **25**(91), 185–188.

The accuracy of references in the text and in this list is the responsibility of the authors, to whom queries should be addressed.

https://doi.org/10.3189/1994AoG20-1-391-396 Published online by Cambridge University Press